Vibrational predissociation of the ArCl2 van der Waals complex: The small molecule limit for intramolecular vibrational redistribution

Nadine Halberstadt, Santiago Serna, Octavio Roncero, and Kenneth C. Janda

Additional information on J. Chem. Phys.

ADVERTISEMENT

Vibrational predissociation of the Ar···Cl₂ van der Waals complex: The small molecule limit for intramolecular vibrational redistribution

Nadine Halberstadt
Laboratoire de Photophysique Moléculaire[a], *Université de Paris Sud, 91405 Orsay, France*

Santiago Serna
Instituto de Física Fundamental, CSIC-UCM, Serrano 123, 28006 Madrid, Spain

Octavio Roncero[b] and Kenneth C. Janda[c]
Department of Chemistry, University of Pittsburgh, Pittsburgh, Pennsylvania 15260

A converged three-dimensional quantum treatment of vibrational predissociation in the $Ar\cdots Cl_2(B\,^3\Pi_{0_u^+},v')$ van der Waals complex is presented. The potential energy surface used is a sum of pairwise Morse atom–atom interactions adjusted asymptotically to a $C_6/R^6 + C_8/R^8$ anisotropic van der Waals form. Calculations have been performed in the energy region of $Ar\cdots Cl_2(B,v' = 6, 10, \text{and } 11)$ excited levels. In agreement with the experimental findings, the final rotational distribution of Cl_2 is found to be strongly dependent on the initial v' state being excited, as well as on the number of vibrational quanta lost in the vibrational predissociation process. The role of intramolecular vibrational redistribution for $v' = 10$ and 11 for which the $\Delta v = -1$ channel is closed is also studied. It is found that the vibrational predissociation (VP) dynamics are dominated by the coupling of the zero-order "bright" state with a single "dark" state from the $v' - 1$ manifold of van der Waals vibrationally excited states which then decays to the continuum, and that the product state distribution is determined by the dissociation of the dark state. This is characteristic of the sparse limit for intramolecular vibrational redistribution. It also implies that the dissociation rate is not governed by a simple function of the initial quantum numbers such as the one given by the energy gap law. The golden rule approximation gives surprisingly accurate results for $Ar\cdots Cl_2$ dynamics. This will be very useful for fitting a potential energy surface to experimental results.

I. INTRODUCTION

The energies and dynamics of van der Waals complexes is a field of considerable interest. In particular, the vibrational predissociation of these molecules provides a clear example of intramolecular energy transfer on a single potential energy surface. The theoretical interpretation[1] of the first experimental studies[2] on He···I₂ has established propensity rules such as the minimum energy or momentum gap law and the minimum transfer of vibrational quanta. Lately, several experimental studies[3–9] have been conducted on electronically excited states of other triatomic systems involving a rare gas atom and a halogen or interhalogen diatomic molecule. These experiments have provided a wealth of detailed information on the dynamics of vibrational predissociation processes: lifetimes and linewidths, spectral shifts, as well as final state vibrational and rotational distributions of the diatomic fragment. A variety of interesting dynamical phenomena were reported. Rainbow and interference effects in the final rotational distribution of the fragments, and intramolecular vibrational redistribution (IVR) prior to dissociation were invoked to explain the results. Time-independent three-dimensional quantum mechanical calculations

on halogen or interhalogen complexes have been conducted for the Rg···Cl₂ (Refs. 3, 4, and 10) and Rg···ICl (Refs. 11 and 12) systems, Rg being a light rare gas atom (He or Ne). From these calculations the following conclusions have emerged: (1) A sum of pairwise atom–atom potentials was able to fit lifetimes as well as final state distributions. (2) The diabatic vibrational golden rule (DVGR) and the rotational infinite order sudden approximation (RIOSA) usually give very good results. (3) The final rotational distribution is not simply determined by the zero-point motion of the quasibound state.

Time-dependent quantum calculations,[13] as well as quasiclassical model calculations,[14] allowed a more detailed interpretation. For example, the quasiclassical model shows the possibility of a rotational rainbow effect, and the quantal time-dependent treatment shows that in the case of He···Cl₂ an interference effect due to the creation of separated wave packets on the final v surface is responsible for the double peak in the final rotational state distribution.

At the other end of the Rg···Cl₂ series, vibrational predissociation of the heavier Xe and Kr complexes[6] leads to a mostly smooth rotational distribution of the Cl₂ fragment, probably due to multiple collisions as the products of vibrational predissociation separate. While vibrational predissociation of these complexes may proceed via an IVR mechanism, rotational collisions in the exit channel lead to statistical behavior.

It is therefore interesting to study the middle member of

the series, namely Ar···Cl_2, for which the van der Waals well depth is of the same order of magnitude as the Cl_2 stretching level spacing. The experiments on the vibrational predissociation of this complex[5] show that the $\Delta v = -1$ channel leads to a smooth but inverted rotational state distribution for the few levels for which this channel is open. For the $\Delta v = -2$ channel, the observed distribution has several local maxima, the position of which is a strong function of the initially excited vibrational level. It was argued that these phenomena could be understood in terms of a sequential relaxation mechansim in which the nature of the intermediate resonance state plays a role in determining the final product energy distribution.

Direct, real time observation of IVR in van der Waals molecules was first performed by Heppener et al. on the Ar···$C_2N_4H_2$ molecule.[15] In the case of Ar···Cl_2 however, a full quantum mechanical treatment of IVR is feasible. In this paper we present a fully converged quantum mechanical calculation for the vibrational predissociation of Ar···Cl_2 excited in the B electronic state, in the region of $v' = 6$ where the $\Delta v = -1$ channel is still open, and in the region of $v' = 11$ where the first open channel is $\Delta v = -2$ ($v = 9$). We use a model potential which is a sum of atom–atom pairwise interactions. The results are in agreement with the main experimental finding that the final rotational distribution is highly structured, and strongly dependent on the initial vibrational level excited. In addition, the product rotational distribution is found to be very different for the different vibrational channels. Since the product rotational distributions due to IVR dynamics are extremely sensitive to the potential energy surface, a fit of the experimental data could provide a very accurate surface for Ar···Cl_2.

Smaller basis set calculations (tested for accuracy against the fully converged results) were performed for $v' = 10$ and 11 to more completely characterize the IVR dynamics. They demonstrate that the $\Delta v = -2$ dissociation dynamics are characteristic of IVR in the sparse limit. This is illustrated in Fig. 1 for dissociation from Ar···Cl_2 ($B,v' = 11$). For Ar···Cl_2, (as was the case for He and Ne···Cl_2), the van der Waals interaction potentials are very similar in the ground and B electronic states. Hence from the ground van der Waals level of Ar···Cl_2 ($X,v'' = 0$) Franck–Condon factors only allow for excitation of the ground level in each van der Waals vibrational manifold associated with level v' of Cl_2 in the B state.

For the case illustrated in Fig. 1, the $v' = 11$ zero-order "bright" state ($B,v' = 11,\mathscr{g}$) corresponds to the ground state $\mathscr{g}$ of the van der Waals vibrational manifold associated with the Ar···Cl_2 B state, Cl_2 stretch $v' = 11$. The $v' = 10$ zero-order "dark" states ($B,v' = 10, \lambda$) correspond to the excited van der Waals levels λ of the Ar···Cl_2 B state, Cl_2 stretch $v' = 10$ manifod that have about the same energy as the $v' = 11$ bright state (but no oscillator strength from the X state, $v'' = 0$). The $v' = 9$ dissocation continua ($B,v' = 9,j,\epsilon$) correspond to the continua of levels of an Ar atom and the Cl_2 ($B,v' = 9$) set of rotational states j, ϵ being the relative translational energy. We find that in the region of $v' = 10$ and $v' = 11$ resonances, the dissociation dynamics are dominated by the mixing of a zero-order bright state
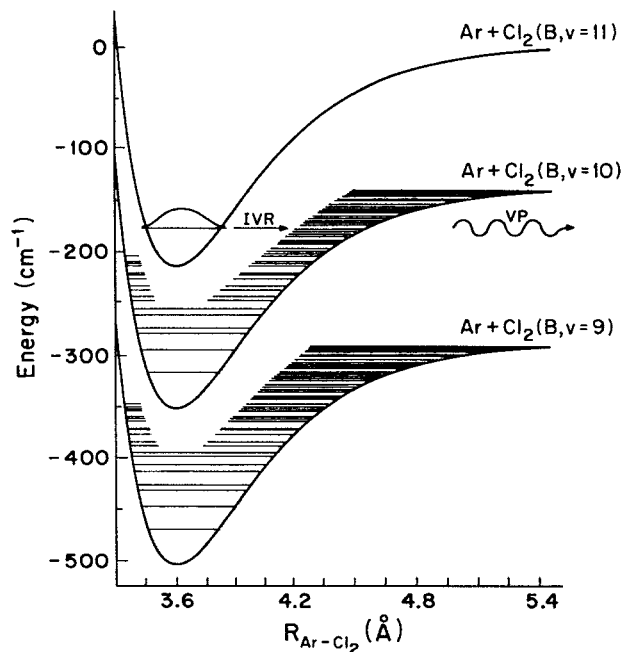

FIG. 1. Enegy level scheme for IVR. This figure provides a one-dimensional representation of the IVR path for Ar···Cl_2. The zero-order bright state (B, $v' = 11,\mathscr{g}$) carries the oscillator strength from the ground state ($X,v'' = 0,\mathscr{g}$). Here B and X refer to the Cl_2 electronic state; v' and v'' refer to the Cl_2 stretch quantum number and $\mathscr{g}$ indicates the ground state of the van der Waals manifold. The dark state, or doorway state, (B, $v' = 19,\lambda$) is a highly excited level, λ, of the van der Waals manifold with a zero-order Cl_2 stretch quantum number equal to 10. The zero-order description of the $\Delta v = -2$ continuum states (B, $v' = 9,\epsilon$) is given by $v' = 9$ for the Cl_2 stretch, j for Cl_2 rotation and ϵ for the translational energy.

($B,v',\mathscr{g}$) responsible for the photon absorption, to a single dark state ($B,v' - 1, \lambda$) of the $v' - 1$ manifold responsible for the dissociation due to its coupling to the $v' - 2$ manifold. In a time-dependent description, this corresponds to the following sequential mechanism. Photon absorption prepares the zero-order bright state ($B,v',\mathscr{g}$), which then decays by IVR to a single dark state ($B,v' - 1, \lambda$), which in turn dissociates to the continuum ($B,v' - 2,j,\epsilon$). For the $v' = 10$ bright state, there is also a slight mixing with a second dark state.

All calculations in this paper are for a total angular momentum $J = 0$, and, as illustrated in the figure, the energy is always relative to that of the van der Waals dissociation limit of the bright state.

The organization of the paper is as follows. Section II presents a summary of the methodology used in the converged calculations. Section III gives the potential for Ar···Cl_2. Section IV presents the calculations, which are discussed in Sec. V in terms of intramolecular vibrational relaxation, while Sec. VI is devoted to conclusions.

II. METHODOLOGY

We have used the method previously described for Ne···Cl_2 (Ref. 10) and Ne···ICl^{12}. This method is based on the calculation of (1) the ground state wave function by

diagonalization in a suitable stretching–bending basis set, (2) the final dissociative wave functions at energy E by integration of a set of rovibrational close-coupled equations with respect to the dissociative coordinate, (3) the overlap between the ground and the final states.

This provides partial and total photofragmentation cross sections at energy E. By varying E around the position of the vibrational predissociation (VP) resonances, the linewidths (and hence the lifetimes) can also be determined. Partial cross sections give the product vibrational and rotational distribution.

We use here the notation of Roncero *et al.*[12] The Hamiltonian for the system is

$$H = -\frac{\hbar^2}{2m}\frac{\partial^2}{\partial R^2} - \frac{\hbar^2}{2\mu}\frac{\partial^2}{\partial r^2} + \frac{l^2}{2mR^2} + \frac{j^2}{2\mu r^2}$$
$$+ V_{Cl_2}(r) + W(r,R,\theta),$$
(1)

where r is the intramolecular distance of Cl_2, R the distance between Ar and the center of mass of Cl_2, and θ the angle between the two vectors $\mathbf{r}$ and $\mathbf{R}$, $m = 2m_{Ar}m_{Cl}/(m_{AR} + 2m_{Cl})$ is the reduced mass for the intermolecular motion corresponding to the potential $W(r,R,\theta)$, $\mu = m_{Cl}/2$ the reduced mass for the intramolecular motion corresponding to the potential $V_{Cl_2}(r)$, and l and j are the two angular momenta associated with $\mathbf{R}$ and $\mathbf{r}$, respectively. Thus j is the quantum number associated with the rotation of the Cl_2 fragment. Note that since Cl_2 is homonuclear, even and odd j's are decoupled. Our calculations only include the even ones, since they give the ground state for $J = 0$.[10]

The initial bound state wave function is expanded as

$$\Psi_i(\mathbf{r},\mathbf{R}) = \sum_{v''}\sum_{n_s'',n_b''} a_{v''n_s''n_b''}^{(i)}\chi_{v''}^{(i)}(r)\chi_{n_s''}^{(i)}(R)\chi_{n_b''}^{(i)}(\hat{r},\hat{R}),$$
(2)

where $\chi_{v''}^{(i)}(r)$ is a basis set of "free" Cl_2 stretch wave functions with energy $E_{Cl_2}^{(i)}(v'')$ obtained by numerical integration of Coxon's Rydberg–Klein–Rees (RKR) potential[16] for the ground electronic state (i) of Cl_2, $\chi_{n_s''}^{(i)}(R)$ a suitable harmonic oscillator basis set for the Ar···Cl₂ stretch, and $\chi_{n_b''}^{(i)}(\hat{r},\hat{R})$ is a van der Waals bending basis function expanded in the $J = 0$ free rotor basis set of the body-fixed system of reference (z parallel to R)

$$\chi_{n_b''}^{(i)}(\hat{r},\hat{R}) = \sum_{j'} b_{n_b''j'}^{(i)} \cdot Y_{j'\cdot 0}(\theta),$$
(3)

where Y_{j0} is a spherical harmonic function and $Y_{j0}(\theta)$ indicates that the other Euler angle has been set to zero hence no integration has to be performed over that angle $[Y_{j0}(\theta) = ((2j + 1)/2)^{1/2}P_\lambda(\cos\theta)]$.

The $b_{n_b''j'}^{(i)}$ are obtained by diagonalizing the angular part of the vibrationally averaged Hamiltonian for a reference vibrational level v_0 at a point R_0 close to the minimum of the well

$$\sum_j \left\{ \left(\frac{\hbar^2 j(j+1)}{2mR_0^2} + E_{v_0,j}^{(i)} - E_{n_b''}^{(i)} \right)\delta_{jj''} \right.$$
$$\left. + \langle j'' | W_{v_0 v_0}^{(i)}(R_0) | j \rangle_\theta \right\} b_{n_b''j}^{(i)} = 0,$$
(4)

with

$$W_{v_0 v_0}^{(i)}(R,\theta) = \langle \chi_{v_0}^{(i)} | W^{(i)}(r,R,\theta) | \chi_{v_0}^{(i)} \rangle_r$$
(5)

and

$$E_{v_0 j}^{(i)} = E_{Cl_2}^{(i)}(v_0) + B_{v_0}^{(i)}j(j+1) - D_{v_0}^{(i)}j^2(j+1)^2,$$
(6)

$B_{v_0}^{(i)}$ and $D_{v_0}^{(i)}$ being the rotational constants of Cl_2 in the vibrational state v_0 of the ground electronic state.[16] A subindex to a bra ket designates the variable with respect to which integration is performed. A final diagonalization of the matrix of the total Hamiltonian (1) in the basis set (2) provides the coefficient $a_{v''n_s''n_b''}^{(i)}$ of expansion (2) and the energies of the van der Waals bound states in the initial ground electronic state.

The final continuum wave function is expanded as follows

$$\Psi_{fvjE}(\mathbf{r},\mathbf{R}) = \sum_{v_c j_c} \phi_{v_c j_c}^{(fvjE)}(R)\chi_{v_c}^{(f)}(r)Y_{j,0}(\theta),$$
(7)

with outgoing asymptotic conditions [Eq. (11) of Ref. (12)]. The vibrational wave functions $\chi_{v_c}^{(f)}(r)$ for Cl_2 in the B excited electronic state (f) are obtained in the same way as the ones for the X state [Eq. (2)]. The coupled equations

$$\left\{ -\frac{\hbar^2}{2m}\frac{\partial^2}{\partial R^2} + \frac{\hbar^2 j(j+1)}{2mR^2} + E_{vj}^{(f)} \right.$$
$$+ \langle Y_{j0} | W_{vv}^{(f)} | Y_{j0} \rangle_\theta - E \left. \right\} \phi_{vj}^{(fvjE)}(R)$$
(8)

$$= -\sum_{v_c j_c \neq vj} \langle Y_{j,0} | W_{v_c v}^{(f)} | Y_{j0} \rangle_\theta \phi_{v_c j_c}^{(fvjE)}(R)$$

were solved using the De Vogelaere integrator.[17] In (8), $E_{vj}^{(f)}$ is the same as $E_{vj}^{(i)}$ of Eq. (6) but for the B electronic state of Cl_2. The partial photodissociation cross section at energy E to produce Cl_2 in the vibrational state v and the rotational state j from the initial ground state $|\Psi_i\rangle$, $\sigma_{fvjE\leftarrow g}$, is taken as the squared overlap of the ground bound state Ψ_i and the continuum Ψ_{vjE} wave function, assuming the transition dipole moment $\mu_0(r)$ to be constant. The total cross section

$$\sigma_{fE\leftarrow i} = \sum_{vj} \sigma_{fvjE\leftarrow i}$$
(9)

provides the photofragmentation line shape as a function of E. Finally, the rotational and vibrational distribution of the fragments is given by

$$P_{vj} = \frac{\sigma_{fvjE\leftarrow i}}{\sigma_{fE\leftarrow i}}.$$
(10)

III. MODEL POTENTIAL FOR THE Ar···Cl₂ MOLECULE

The intermolecular potential energy surface used in this work to describe the Ar···Cl₂ molecule is similar to the ones used for Ne···Cl₂ (Ref. 4) and He···Cl₂, and to the ones used by Reid *et al.*[18] to calculate the bound states of He, Ne, and Ar···Cl₂. In the region of the well it is a sum of atom–atom pairwise interactions, and it is adjusted to an anisotropic van der Waals form in the asymptotic region

$$W = \begin{cases} V_M & \text{if } R \leqslant R_i, \\ V_{vdw} + (V_M - V_{vdw})f & \text{if } R \geqslant R_i, \end{cases}$$
(11)

with

$$V_M(r,R,\theta) = V_{\mathrm{ArCl}}(R_{\mathrm{ArCl}_a}) + V_{\mathrm{ArCl}}(R_{\mathrm{ArCl}_b}),$$

$$V_{\mathrm{vdw}}(R,\theta) = C_6(\theta)/R^6 + C_8(\theta)/R^8, \qquad (12)$$

$$f(R) = e^{-\rho[(R-R_i)/(\tilde{R}_{\mathrm{ArCl}})]^2},$$

where $\tilde{R}_{\mathrm{ArCl}}$ is defined in the next equation. $V_{\mathrm{ArCl}}(R_{\mathrm{ArCl}})$ in Eq. (12) is described by a Morse function

$$V_{\mathrm{ArCl}}(R_{\mathrm{ArCl}}) = D\{e^{-2\alpha(R_{\mathrm{ArCl}} - \tilde{R}_{\mathrm{ArCl}})} - 2e^{-\alpha(R_{\mathrm{ArCl}} - \tilde{R}_{\mathrm{ArCl}})}\},$$

$$(13)$$

where the distances R_{ArCl} between pairs of atoms are related to r, R, and θ by

$$R_{\mathrm{ArCl}} = \sqrt{R^2 + (r/2)^2 \pm Rr\cos\theta}. \qquad (14)$$

The parameters D and $\tilde{R}_{\mathrm{ArCl}}$ for the Morse potential have been obtained by a rough adjustment to the available experimental data (dissociation energy and equilibrium distance), by performing a bound state caculation similar to that giving the ground state of the complex [Eqs. (2)–(6)] but for the quasibound state $(B, v' = 6, \mathscr{g})$. The parameter α was taken from Ref. 18. Since the experimental spectra show no van der Waals progressions, we have taken for simplicity the same intermolecular parameters for the ground and excited electronic states.

The van der Waals potential V_{vdw} in Eq. (12) includes anisotropy through the angular dependence of the C_6 and C_8 coefficients[18]

$$C_n(\theta) = C_{n0} + C_{n2}P_2(\cos\theta). \qquad (15)$$

The intramolecular potential V_{Cl_2} was obtained by cubic spline interpolation of Coxon's RKR potential,[16] adding the equilibrium distance[19] [$r_e = 2.4311$ Å, $V_{\mathrm{Cl}_2}(r_e) = -0.182$ cm^{-1} in the B state, $r_e = 1.9880$ Å, $V_{\mathrm{Cl}_2}(r_e) = 0$ cm^{-1} in the X state].

All the potential parameters used in the calculations are given in Table I. The following masses were used in the calculations: $m_{\mathrm{Ar}} = 40$ amu and $m_{\mathrm{Cl}} = 35$ amu.

The matrix elements of the potential $\langle Y_{j'0}|W_{v'v}^{(l)}|Y_{j0}\rangle_\theta$ were calculated analytically using a Legendre expansion on a grid of 50 unequally spaced points between 2.5 and 13.0 Å with cubic spline interpolation between the points and a $C_6/R^6 + C_8/R^8$ extension beyond 13.0 Å when necessary.

In Fig. 2 we present a contour plot of the intermolecular potential, averaged over the vibrational wave function $v' = 11$ of Cl$_2$. The equipotentials are 50 cm^{-1} apart. The minimum is at the perpendicular configuration, with $R_e = 3.6$ Å and $W_{11,11}^{(l)}(R_e,\pi/2) = -208.1$ cm^{-1}. The average position of the chlorine atoms for $v' = 11$ is also represented.
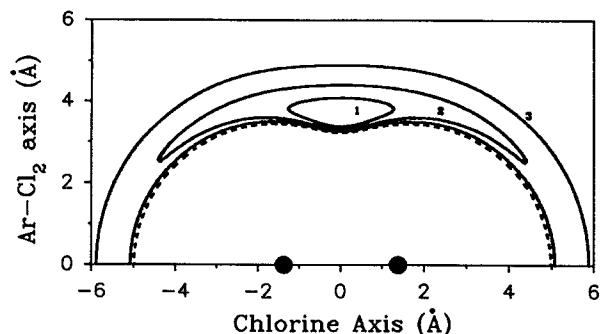

FIG. 2. Contours of $W_{11,11}^{(l)} = \langle v' = 11|W|v' = 11\rangle_r$, the van der Waals potential for Ar⋯Cl₂ averaged over the Cl₂ vibrational motion for the (B, $v' = 11$) level. (1) -150 cm^{-1}; (2) -100 cm^{-1}; (3) -50 cm^{-1}. Also shown is the equipotential $W_{11,11}^{(l)} = 0$ on the repulsive wall. The minimum of the well is at $\theta_e = \pi/2$ (perpendicular configuration), with $R_e = 3.6$ Å and $W_{11,11}^{(l)}(R_e,\theta_e) = -208.1$ cm^{-1}. The two Cl atoms are represented at their average position for $v' = 11$.

IV. RESULTS

A. Ground state

The bound state Ar⋯Cl₂$(X,v'' = 0)$ was calculated with 15 harmonic oscillator wave functions (frequency $= 37.9$ cm^{-1}, equilibrium distance $= 3.7$ Å), and 10 bending functions obtained from 20 spherical harmonics at $R_0 = 3.7$ Å, using 20 Legendre polynomials in the expansion of the potential. A convergence study showed that only one vibrational function ($v = 0$) of Cl₂ was needed. The resulting energy was -179.29787 cm^{-1} with respect to the Ar + Cl₂$(X,v = 0)$ dissociation limit.

B. Converged calculations: Position and width of the resonances

We have conducted full three-dimensional photofragmentation cross section calculations for Ar⋯Cl₂ in the spectral region corresponding to the $B \leftarrow X$ transition of the Cl₂ moiety. Integration of the close-coupled equations was performed from 3.0 to 20.0 Å with a step of 0.002 Å. As expected, when the energy of the photon is varied, narrow lines are found in the near vicinity of the quasibound van der Waals levels, which are broadened by vibrational predissociation.

The resonances were first approximately localized by calculating the corresponding quasibound state [Ar⋯Cl₂$(v' = 11)$ or $(v' = 6)$] using the same proceedure as for the ground state, including only one v' in the basis. Then calculation of the cross section at three values of the

TABLE I. Ar⋯Cl₂(B) potential energy surface parameters used in the calculations.

$D = 106$ cm^{-1}	$\alpha = 1.8$ Å^{-1}	$\tilde{R}_{\mathrm{ArCl}} = 3.9$ Å
$\rho = 4$	$R_i = \tilde{R}_{\mathrm{ArCl}} + \ln 2/\alpha = 4.285$Å	
$C_{60} = -923\,000$ cm^{-1} Å^6		$C_{62} = -140\,000$ cm^{-1} Å^6
$C_{80} = -9\,050\,000$ cm^{-1} Å^8		$C_{82} = -3\,620\,000$ cm^{-1} Å^8

energy around the quasibound state allowed a good localization of the resonance (assuming a Lorentzian shape, which was later checked by calculating a few more points).

Figure 3 presents the total cross section calculated as a function of energy for the photofragmentation of Ar···Cl₂ in the region of the $(B,v' = 6,\mathscr{g})$ and the $(B,v' = 11,\mathscr{g})$ resonances. Each resonance has a Lorentzian line shape, with total width $2\Gamma = 2.06 \times 10^{-3}$ cm^{-1} for $v' = 6$ and 2.11×10^{-2} cm^{-1} for $v' = 11$, corresponding to lifetimes for vibrational predissociation of $\tau = \hbar/2\Gamma = 2.6$ ns and 251 ps, respectively. The resonances are centered at $E = -178.288\,20$ cm^{-1} below the Ar + Cl₂$(B,v' = 6)$ limit and $E = -176.603\,04$ cm^{-1} below the Ar + Cl₂$(B,v' = 11)$ limit. For comparison, the quasibound states were found at $-178.322\,11$ cm^{-1} for $v' = 6$ and $-176.976\,38$ cm^{-1} for $v' = 11$. Note that although the $\Delta v = -1$ dissociation channel for Ar···Cl₂$(B,v' = 6,\mathscr{g})$ is open with only 17.8 cm^{-1} excess kinetic energy, vibrational predissociation for this level is about ten times slower than for Ar···Cl₂$(B,v' = 11,\mathscr{g})$ where $\Delta v = -1$ is closed and dissociation via $\Delta v = -2$ releases 117.6 cm^{-1} excess kinetic energy. The failure of the calculated VP rates to obey the energy gap law is due to IVR and is discussed in Sec. V.

C. Converged calculations: Rotational distributions

Using Eq. (10) we have calculated the rotational distributions for the Cl₂ fragments originating from Ar···Cl₂$(B,v' = 6,\mathscr{g})$ and dissociating via $\Delta v = -1$ and -2 to $v = 5$ and $v = 4$, and for Cl₂ fragments originating from Ar···Cl₂$(B,v' = 11,\mathscr{g})$, dissociating via $\Delta v = -2$ and -3 to $v = 9$ and $v = 8$. The results are presented in Tables II and III. For $v' = 6$, five vibrational channels were
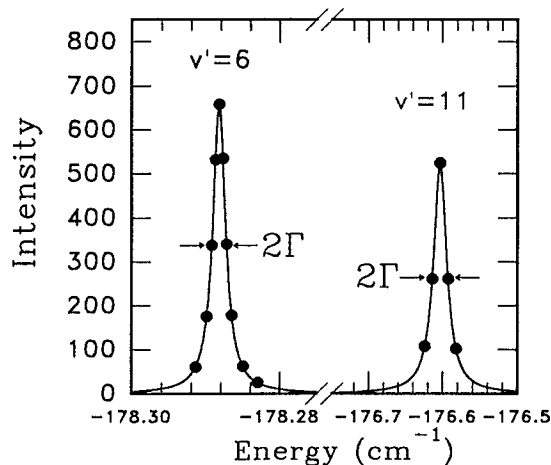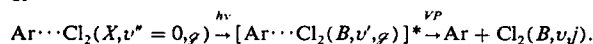
TABLE II. Calculated rotational distributions of Cl₂ fragments in the vibrational predissociation of Ar···Cl₂$(B,v' = 6,\mathscr{g})$.

| | | $\Delta v = -1$ | | | $\Delta v = -2$ | | |
		Converged calculation	$|\Delta v| > 1$ coupling cut off	Golden rule calculation	Converged calculation	$|\Delta v| > 1$ coupling cut off	Golden rule calculation
	Σ	81.9813	80.0779	71.5004	17.7376	19.5576	28.0539
$j =$	0	17.9434	17.7665	16.4066	2.2930	2.3954	1.5213
	2	13.6027	13.2588	5.0537	2.9060	3.0503	1.8617
	4	20.9268	20.8179	14.7539	3.0119	3.1795	2.4438
	6	19.3767	19.5399	20.6402	4.3715	4.5345	3.3691
	8	22.4161	22.8791	36.9621	3.9576	4.1943	3.8092
	10	5.7343	5.7377	6.1835	4.9010	5.1575	4.4959
	12				5.8414	6.0431	6.3421
	14				7.7556	7.8700	7.6189
	16				4.8324	5.0148	5.2389
	18				4.7515	4.8884	5.1565
	20				9.1135	9.0984	9.0685
	22				8.2199	8.1825	9.4599
	24				7.6189	7.4458	7.9878
	26				6.8832	6.6546	6.9076
	28				5.7267	5.5335	6.5736
	30				7.2637	6.8655	6.7687
	32				3.0647	2.8973	4.1442
	34				6.3812	5.9717	5.8474
	36				1.1063	1.0228	1.3850
	38				0	0	0

FIG. 3. Total absorption cross section obtained in the line shape calculation of

$$\text{Ar}\cdots\text{Cl}_2(X,v'' = 0,\mathscr{g}) \xrightarrow{h\nu} [\text{Ar}\cdots\text{Cl}_2(B,v',\mathscr{g})]^* \xrightarrow{VP} \text{Ar} + \text{Cl}_2(B,v,j).$$

a: $v' = 6$; b: $v_1 = 11$. The points are the results of the converged three-dimensional calculation, and the curve is a Lorentzian fit to the calculated points giving the resonance energy E_0 and width, full width at half maximum (FWHM) 2Γ corresponding to a lifetime $\tau = \hbar/2\Gamma$ for the quasibound state [Ar···Cl₂(B,v', g)]*. For $v' = 6$, $E_0 = -178.2882$ cm^{-1}, $2\Gamma = 2.1 \times 10^{-3}$ cm^{-1}, $\tau = 2.6$ ns; for $(v' = 11)$, $E_0 = -176.603$ cm^{-1}, $2\Gamma = 2.1 \times 10^{-2}$ cm^{-1}, and $\tau = 250$ ps.

TABLE III. Calculated rotational distribution of Cl₂ fragments in the vibrational predissociation of Ar···Cl₂$(B,v' = 11,\mathscr{g})$.

| | | $\Delta v = -2$ | | $\Delta v = -3$ | |
		Converged calculation	Golden rule calculation	Converged calculation	Golden rule calculation
	Σ	90.2120	90.9505	8.8715	8.5461
$j =$	0	4.6892	4.4282	1.2445	1.0077
	2	0.7573	1.8681	1.9042	2.0722
	4	2.1924	0.7766	7.6103	6.2357
	6	0.9384	0.0188	5.7526	6.1260
	8	3.0822	4.5159	2.7418	1.8496
	10	27.0754	24.6689	2.9889	0.7293
	12	13.4773	14.6311	6.1488	14.7413
	14	0.2885	0.1852	18.6421	17.7679
	16	2.4087	2.2919	8.2988	4.8669
	18	1.6852	3.9985	2.6615	3.8512
	20	7.9769	5.1024	10.1222	8.9835
	22	8.5509	7.0925	3.7090	5.2595
	24	13.0533	13.2840	7.8671	7.1813
	26	9.4169	12.6616	2.5593	2.9339
	28	4.4072	4.4763	0.8810	0.8205
	30			6.5729	6.3138
	32			7.1707	6.3726
	34			0.5716	0.8692
	36			0.7794	0.4725
	38			1.0696	0.7550
	40			0.5932	0.7251
	42			0.1104	0.0652
	44			0	0

needed to get convergence for the rotational distributions corresponding to $\Delta v = -1$ and $\Delta v = -2$ (120 channels total[20]). For $v' = 11$, six vibrational channels ($v = 7$–12) were needed to get convergence for $\Delta v = -2$ (180 channels total[21]), and 8 vibrational channels were necessary (from $v = 6$–13) for $\Delta v = -3$ (210 channels total[22]). The convergence on the rotational distributions was then better than 0.5%.

The converged rotational distributions are plotted in Figs. 4 and 5, together with the experimental results from Ref. 5 for the first open channel.

The calculated rotational distributions are quite different from the measured ones. This is probably due to inaccuracy in the anisotropy of the assumed potential. Still, the qualitative observations of highly structured rotational distributions that are quite different for different initial Cl$_2$ vibrational levels are reproduced in the calculations. This will be even more evident in the next section in which results for $v' = 10$ and 11 are compared. Unfortunately, the experimental distributions for $\Delta v = -2$ dissociation of $v' = 6$ and $\Delta v = -3$ dissociation of $v' = 11$ were not measured. For $v' = 11$ it was estimated that the $\Delta v = -3$ dissociation accounts for less than 10% of the total. This is consistent with the 9% calculated probability for $\Delta v = -3$.

D. Smaller basis set calculations: IVR resonances

Each point of the fully converged $v' = 11$ calculations required four hours of central processing unit (CPU) time
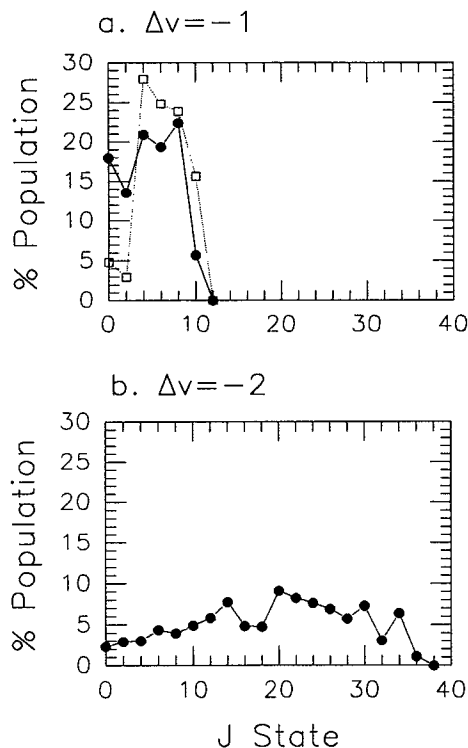

a. $\Delta v = -1$

b. $\Delta v = -2$

FIG. 4. Cl$_2$(v) rotational distribution for (a) $\Delta v = -1$ and (b) $\Delta v = -2$ dissociation from the $v' = 6$ level. The solid circles are the results of the converged calculation and the open squares are the experimental results of Ref. 5.

a. $\Delta v = -2$

b. $\Delta = -3$

FIG. 5. Cl$_2$(v) rotational distribution for (a) $\Delta v = -2$ and (b) $\Delta v = -3$ dissociation from the $v' = 11$ level. The solid circles are the results of the converged calculati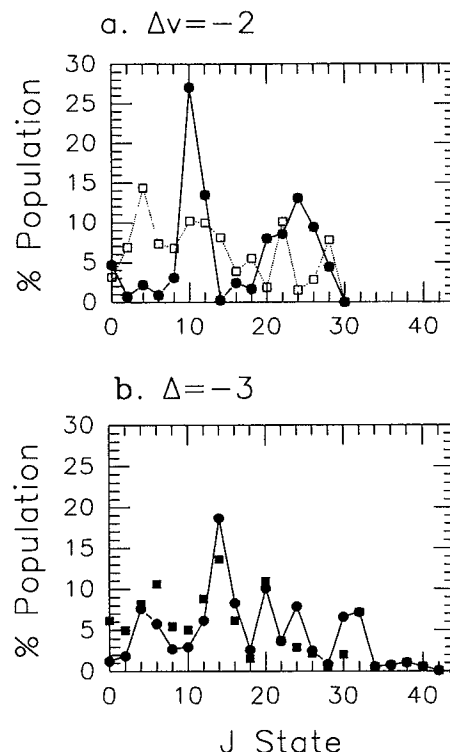on. The open squares are the experimental results of Ref. 5. (The measured distribution depends on the initial rotational state of the complex, and may be more structured for a state-selected experiment). The solid squares show the result of a golden rule calculation for the doorway state, as described in Sec. V B. (Most of the solid circles and squares are superposed and not distinguishable.)

on the Fujitsu VP200 computer at Orsay. Therefore we were not able to perform extensive searches for the dark states that couple with the final state of the principal transition. Such calculations were performed for $v' = -10$ and 11 employing a smaller basis of 5 Cl$_2$ stretching levels and 150 total channels.[23] These calculations reproduce the converged calculations. For instance the $v' = 11$ bright resonance for the reduced basis is at -176.599 cm^{-1} compared to -176.603 cm^{-1} for the converged calculation. Similarly, the rotational distributions display the same pattern as those of the converged calculation although the probability of any given channel may be in error by 1% (the rotational distribution corresponding to the first open vibrational channel is quite well converged). For each energy the smaller basis set calculations required about 2 h on the FPS 500-EA or 1 h on the VAX 9000 vector processor computer at the University of Pittsburgh. (The CPU times given here are only rough approximations of the time required to perform the calculations: no extensive effort was made to optimize the code.)

Figures 6 and 7 show 2 cm^{-1} wide spectra in the region of the principal transitions for $v' = 11$ and 10, respectively. A weak transition is observed 1.03 cm^{-1} to lower energy of the principal resonance for $v' = 11$. Although the peak intensity of this "dark" state transition is 1/50 times that of the bright state transition, its width is 9 times greater so that the
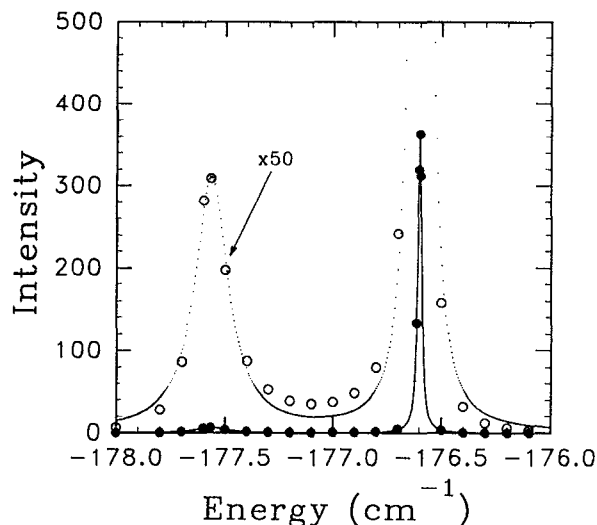
FIG. 6. A 2 cm^{-1} wide search in the region of the $(B, v' = 11, \mathscr{G})$ bright state reveals a single dark state whose integrated intensity is 15% of that of the bright state. Quasibound state calculations enable us to assign this as mainly due to the $(B, v', = 10, \lambda = 29)$ level. The parameters that summarize the widths and intensities of these transitions are given in Table V(c).

integrated intensity is 15% of the principal transition.

As shown in Fig. 8(a), the product rotational distributions for decay of the bright and dark states are very similar. These phenomena are consistent with a zero-order picture of a $v' = 11$ bright state that decays to the $\Delta v = -2$ continuum by coupling with a single highly excited van der Waals mode in the $\Delta v = -1$ manifold.

In Fig. 7, three resonances are observed in the region of the transition to the zero-order $v' = 10$ state. The transition
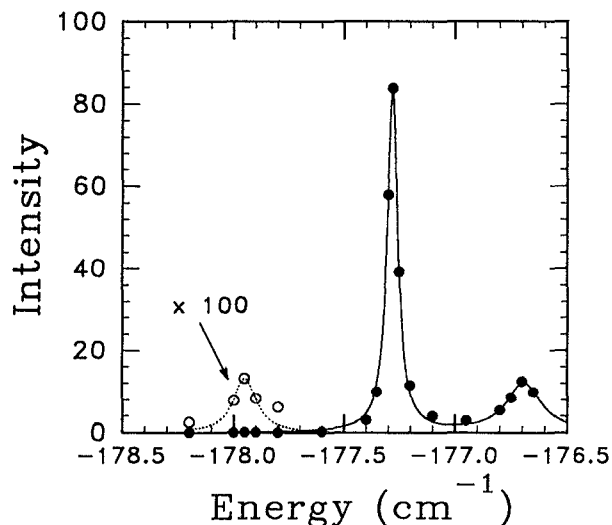

FIG. 7. A 2 cm^{-1} wide search in the region of the $(B, v' = 10, \mathscr{G})$ bright state reveals two dark states. The more strongly mixed dark state borrows 30% of the total intensity. Quasibound state calculations yield a zero-order assignment for this state as $(B, v' = 10, \lambda = 36)$. The other dark state borrows less than 1% of the total intensity, and is mainly $(B, v' = 10, \lambda = 35)$. Parameters for the bright and the more intense dark state are given in Table V(b).

to a dark state 0.6 cm^{-1} higher in energy than the principal transition is quite intense. Its integrated intensity is 43% that of the principal transition. The third observed transition is less than 1% as intense as the two other transitions.

As shown in Fig. 8(b), the two relatively intense transitions yield quite similar product rotational distributions while the weak transition leads to a qualitatively different product state distribution. Thus the $v' = 10$ zero-order state couples strongly with one dark state and weakly to another. Although there may be other dark states in the region of these resonances, they do not couple strongly enough to the bright states to be observed. As expected from the experimental results, the $v' = 11$ and $v' = 10$ bright state resonances lead to very different product rotational distributions. Unfortunately, the transitions corresponding to the dark resonances could not be seen in Ref. 5 because the experimental resolution did not allow for single state excitation due to spectral congestion in the absorption of the Ar···Cl$_2$ complex. This should be feasible with an increased frequency resolution of the exciting laser.

V. DISCUSSION

The discussion section starts with an overview of the motivation of this work and the results which were obtained,
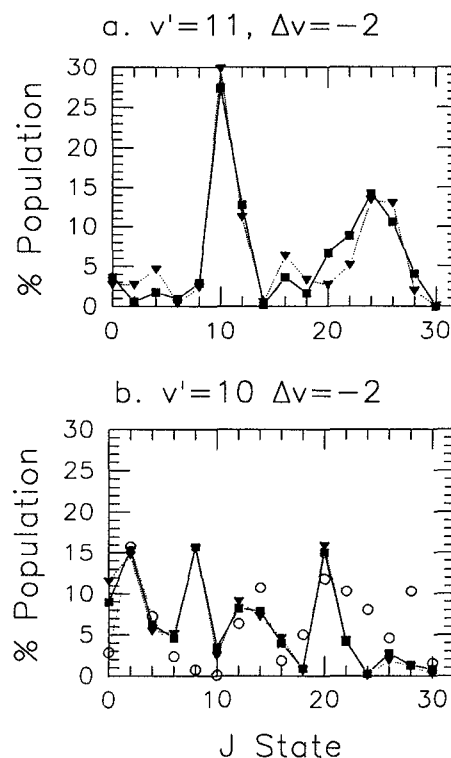
FIG. 8. Rotational distributions calculated for (a) the bright $(B, v' = 11, \mathscr{G})$ (solid squares) and dark $(B, v' = 10, \lambda)$ (solid triangles) state resonances of Fig. 6: since the two distributions are so similar, it appears that the dissociation dynamics are completely controlled by the dark state (note that 54% of the total goes into $j = 10$, 12 and 24); (b) the bright $((B, v' = 10, \mathscr{G})$ (solid squares) and dark $(B, v' = 9, \lambda)$ (solid triangles and open circles) state resonances of Fig. 7: the bright state and the more strongly mixed dark state $(\lambda = 36)$ yield the same rotational distribution, while the weakly mixed dark state yields quite a different distribution.

and then presents the detailed analysis of the dissociation mechanism, the initial, intermediate, and final state wave functions, the IVR resonances, the validity of approximate treatments, and the possibility of combining theory with experiment for a precise determination of the potential for $Ar \cdots Cl_2$.

These calculations are motivated by a hypothesis that $\Delta v = -2$ vibrational predissociation of $Ar \cdots Cl_2$ occurs via a sequential IVR process rather than by direct coupling of the initially excited quasibound state to the dissociative continuum. The direct coupling mechanism has usually been assumed for triatomic van der Waals molecules, and is the basis for the energy gap and momentum gap laws[1] that are very useful for understanding the vibrational predissociation dynamics when $\Delta v = -1$ dissociation is allowed. This is the case for $He \cdots Cl_2$, $Ne \cdots Cl_2$, and other species for which the van der Waals bond energy is less than the energy of a single vibrational quantum of the covalent mode. The IVR mechanism was proposed for $Ar \cdots Cl_2$ because the product rotational distributions for vibrational predissociation are highly structured and are quite different for each initially excited vibrational level. This is in contrast to dissociation of $He \cdots Cl_2$, for instance, for which the product rotational distributions are smooth and remarkably independent of either the initially excited vibrational level and whether the final vibrational level corresponds to $\Delta v = -1$, -2, or -3. The calculations reported here give conclusive evidence for the IVR mechanism of $\Delta v = -2$ dissociation of $Ar \cdots Cl_2$.

Fully converged three-dimensional calculations were performed for the resonance widths and product state distributions for the $v' = 6$ and 11 levels of the $Ar \cdots Cl_2$ B state. To investigate the importance of higher order coupling, the calculations were repeated for the $v' = 6$ level except that all direct $|\Delta v| > 1$ coupling was suppressed. Similar calculations were performed for $Ne \cdots Cl_2$ ($v' = 11$) for comparison, and are discussed in Sec. V A below.

In order to show that vibrational predissociation from the $v' = 11$ level of $Ar \cdots Cl_2$ proceeds via a resonance with an intermediate metastable state, the continuum ($v < 11$) wave function in the region of the resonance was analyzed by calculating its overlap with the quasibound $v' = 11$ level multiplied by the coupling between them. This gives a measure of the localization of the continuum wave function in the region of the well, hence a way of looking for the intermediate metastable state. For comparison, this procedure was repeated for the $v' = 6$ level for which no IVR occurs since $\Delta v = -1$ is an open channel.

The converged calculations for the $v' = 6$ and 11 levels show that, for the assumed potential energy surface, it is now possible to obtain an exact solution of the vibrational dynamics of $Ar \cdots Cl_2$. Previously this has been difficult since the well depth for this molecule is deep enough that the Cl_2 stretch levels can no longer be treated by perturbation theory such as a golden rule calculation and a large basis set must be used to integrate the continuum state for an exact line shape calculation. The results obtained from the converged calculations are qualitatively in accord with the experimental results. The lifetimes of the $v' = 6$ and 11 levels are, respectively, 2.6 ns and 251 ps. These are long enough that

experimental line broadening measurements would not be possible for the laser resolution employed in Ref. 5. Although the calculated distributions are quite different in detail from those observed, they are highly structured for $\Delta v = -2$ dissociation, and quite sensitive to both the initial value of v' and the number of quanta lost during dissociation. For dissociation from the $v' = 6$ level (Fig. 4), the $\Delta v = -1$ product rotational distribution is relatively smooth, and each allowed product rotational level is observed. The $\Delta v = -2$ distribution is also relatively smooth. In contrast, dissociation from the $v' = 11$ level (Fig. 5) produces a highly structured rotational distribution for $\Delta v = -2$, with over 50% of the products in the $j = 10$, 12, and 24 states, while $j = 14$, for instance, accounts for less than 1% of the products. The rotational distribution for $\Delta v = -3$ also is predicted to be quite structured, and quite different from that of $\Delta v = -2$.

Finally, we looked for the IVR resonances. If the dynamics for $Ar \cdots Cl_2$ fall within the sparse limit for IVR, then the oscillator strength to the zero-order bright state, ($v' = 11, \mathscr{G}$) for instance, should be distributed among the eigenstates according to the proportion of ($v' = 11, \mathscr{G}$) mixed into the eigenstates. Then at least two resonances should be seen in the same energy region, revealing the existence of any zero-order dark states that interact with the bright state. For this purpose we performed smaller basis set calculations (150 channels), that were converged to within 1% of the full calculations for the $\Delta v = -2$ product state distribution. With the smaller basis, we were able to search for weak resonances, and found one in the region of the $v' = 11$ bright state, and two in the region of the $v' = 10$ bright state. In Sec. V B, these resonances will be discussed within the framework of the IVR mixing model, and the dark states will be compared to quasibound state calculations of the levels that correspond to these resonances. This allows us to tentatively assign the dark states to specific levels within the van der Waals manifold. In addition, a golden rule calculation of the dark state dissociation shows that, in agreement with the IVR model, the final Cl_2 rotational distribution is governed by that state.

The relative VP rates for the three levels which were studied are quite different from what would be predicted from the energy gap law. The $v' = 6$ level, with a $\Delta v = -1$ energy gap of only 18 cm^{-1}, has a lifetime of 2.5 ns while the principal $v' = 11$ level with a $\Delta v = -2$ energy gap of 118 cm^{-1} has a lifetime of only 250 ps. The decay rates for the $v' = 10$ and $v' = 11$ bright states depend on the strength of the coupling to nearby dark states, which does not correlate with v'. Another important result is that each bright state and the dark state to which it is most strongly coupled leads to the same product rotational distribution.

A. Sequential or direct mechanism

The measured features of the product state distribution discussed in the previous section lead Evard *et al.*[5] to postulate that $Ar \cdots Cl_2$ dissociates via an IVR mechanism. They argued that the sharp features in the rotational distributions upon $\Delta v = -2$ dissociation are due to the retention of the

bending mode character of the $\Delta v = -1$ resonant state. Since the intermediate state that is in resonance with the initial quasibound state would be expected to be different for each Cl$_2$ stretch level, v', a different product distribution would be expected for each initially excited v' level. We have attempted to analyze this hypothesis in two ways. First, the close-coupling results are analyzed for the nature of the initial quasibound state and the product continuum using golden rule basis sets. Second, the relative importance of $|\Delta v| = 1$ and $|\Delta v| > 1$ coupling terms in the potential that lead to dissociation was investigated.

1. Characterization of the continuum: Golden rule calculations

We present here the analysis of the continuum wave functions. A golden rule type calculation was performed to obtain the extent of overlap of the product continuum state with the initial quasibound level. A coupling cross section vs energy was calculated using Eq. (16).

$$\Gamma(E) = \sum_{vj} \Gamma_{vj}(E),$$
$$\Gamma_{vj}(E) = \pi |\Psi_{fvjE}^{(0)} | \mathscr{W} | \Psi_i^0 \rangle|^2. \tag{16}$$

Here $\Psi_i^{(0)}$ is the quasibound state function with energy $E_i^{(0)}$ expanded as in Eq. (2) except that only the specified v' level (either 6 or 11) is used in the expansion. $\Psi_{fvjE}^{(0)}$ is the continuum wave function that coresponds to Ar + Cl$_2(B, v < v', j)$ in the asymptotic limit, and is expanded as in Eq. (7) except that only the vibrational wave functions with $v_c < v'$ are used. Since the quasibound state function is localized within the well, and since $\mathscr{W}$ (the coupling potential) also is mainly localized near the well, $\Gamma(E)$ should vary slowly with energy unless the continuum function is also localized near the well region. If $\Gamma(E)$ does vary with energy, then this corresponds to a resonance for the $v < v'$ continua.

The results of this calculation are shown in Fig. 9. For the $v' = 6$ quasibound state, only a slowly varying cross section is observed: there is no indication of a resonance. For the $v' = 11$ quasibound state a resonance 0.14 cm^{-1} wide, located 0.36 cm^{-1} below the exact resonance is obtained. This indicates that the $v' = 6$ level decays by a direct coupling to the continuum while the $v' = 11$ state undergoes IVR in the small molecule limit of coupling to a specific intermediate level. This conclusion is further supported by the fact that the product rotational state distribution for vibrational predissociation of Ar···Cl$_2(v' = 6)$, calculated by the golden rule method (given in Table II), is surprisingly similar to that of the exact calculation even though there is extensive mixing in the Cl$_2$ stretching basis.

It is interesting to note that the width of the Lorentzian in Fig. 9(b) is much larger than the actual width of $v' = 11$ resonance. This is because the bound levels ($v' = 10, \lambda$) of the $v' = 10$ channel are directly coupled to the continuum $\Delta v = -1$, while the ($v' = 11, \mathscr{G}$) quasibound level is only indirectly coupled to the same continuum by its mixing with the bound levels of the $v' = 10$ channel. In addition, the ($v' = 10, \lambda$) levels contain some excitation energy in the
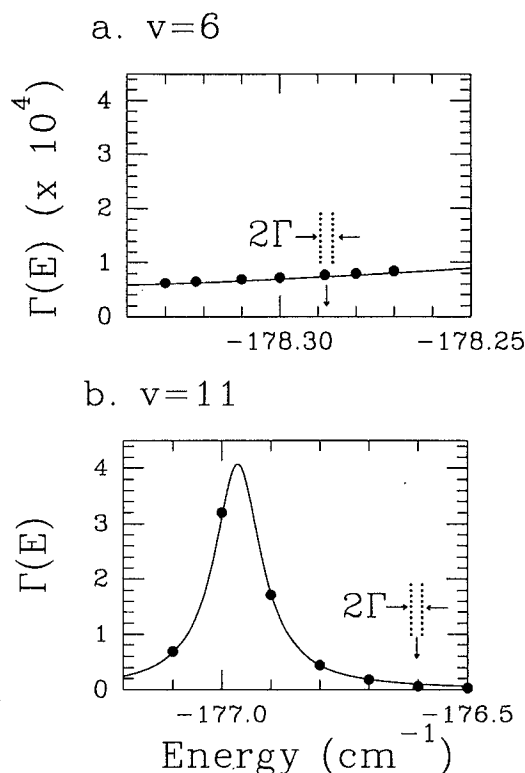

FIG. 9. The golden rule coupling $\Gamma(E)$ of the (a) ($B, v' = 6, \mathscr{G}$) and (b) ($B, v' = 11, \mathscr{G}$) quasibound states to the continuum $v < v'$ as defined by Eq. (16), as a function of energy. $\Gamma(E)$ is a measure of the localization of the continuum ($v < v'$) function in the region of the well. The lack of a resonance for the $v < v' = 6$ state shows that there is no continuum state with a strong localization at the configuration of the quasibound state ($v' = 6, \mathscr{G}$). For $v' = 11$, there is such a localization, corresponding to the zero-order "dark" state ($v < v' = 11, \lambda$). Remarkably, the golden rule calculation gives a good estimation of the dark state width and of the rotational distribution. The position of the resonance in the line shape calculation is indicated by a vertical arrow and its width is delimited by two horizontal arrows.

stretching van der Waals mode, which is the dissociative coordinate. It is remarkable that the golden rule treatment yields the same resonance width as the line shape calculation for the dark state resonance, Fig. 6, although it does not give the correct position of the resonance since it neglects the $W_{10,11}^{(f)}$ bound–bound coupling terms.

It is also interesting that the golden rule treatment gives quite accurate product state distributions for the $v' = 11$ bright state (Table III). As will be described more completely in the next section, a separate golden rule calculation was performed to obtain the product state distribution for the ($v' = 10, \lambda = 29$) dark state. As shown in Fig. 5, the results of this calculation are in remarkable agreement with the exact calculation of the ($v' = 11, \mathscr{G}$) bright state product rotational distribution. The success of the golden rule is probably due to the fact that IVR is mainly due to bound–bound interactions between the v' and $v' - 1$ potentials, but the bound–continuum interaction responsible for vibrational predissociation remains weak (the lifetime of the quasibound state is several hundred times the Cl$_2$ vibrational period), and so does the continuum–continuum interaction (the one between $v' = 11$ and $v' = 10$ is neglected in the golden rule

calculation). Also, even though the bright and dark states are significantly mixed, the two resonances in Figs. 6 and 7 are still separated by 100 times the bright state resonance width, and the states may be considered to be isolated. This is confirmed by the Lorentzian profile obtained in the spectrum calculation.

2. Role of the $\Delta v = \pm 1$ coupling

For collisional vibrational relaxation transitions corresponding to $|\Delta v| > 1$ proceed via $\Delta v = \pm 1$ coupling. In our case, this coupling corresponds to $W_{v,v \pm 1}^{(f)}$ ($= W_{v \pm 1,v}^{(f)}$). To investigate further the specific couplings that lead to dissociation of the van der Waals complexes, we have repeated the spectrum calculation while selectively deleting from Eq. (8) any $W_{v',v}^{(f)}$ coupling term with $|v - v'| > 1$. Tables II and IV give the results of such calculations for Ar···Cl$_2(v' = 6)$ and for Ne···Cl$_2(B,v' = 11)$.

For the Ne···Cl$_2$ calculation, deletion of the $|\Delta v| > 1$ coupling terms has no effect on the $\Delta v = -1$ rotational distribution or on the $\Delta v = -1/\Delta v = -2$ branching ratio, and only a small effect on the $\Delta v = -2$ distribution. Similar results are obtained for Ar···Cl$_2(v' = 6)$. The rotational distribution for the first open channel is essentially unchanged, slight changes occur for $\Delta v = -2$ and -3. In addition the resonance energy is shifted by 0.001 cm^{-1} and the $\Delta v = -1/\Delta v = -2$ branching ratio changes by 2%.

Thus the $\Delta v = \pm 1$ coupling is mainly responsible for all the transitions corresponding to vibrational predissociation: the influence of direct $\Delta v = \pm n$ with $n > 1$ coupling is negligible. This shows that in a time-dependent picture, the mechanism for losing more than one vibrational quantum of

Cl$_2$ is sequential, proceeding through several $\Delta v = -1$ steps.

Another important consequence of this result is that the calculation of the potential matrix can be appreciably reduced when the number of vibrational channels involved is large: the factor is $n_v (n_v + 1)/2(2n_v - 1) \simeq n_v/4$ if n_v is the number of vibrational channels and if they each have about the same number of rotational channels.

B. Direct calculation of the IVR resonances

With the smaller basis set calculations presented in Sec. IV D we were able to make a direct search for the IVR resonances. For both $v' = 11$ and 10 (Figs. 6 and 7), a single dark state was found to be significantly mixed with the bright state. In each case the bright state resonance is significantly narrower than that of the dark state, while the bright state and the associated dark state lead to the same product rotational distribution (Fig. 8). The weakly mixed dark state for $v' = 10$, however, leads to quite a different product state distribution. These phenomena are in accord with the IVR model in which the bright state contributes oscillator strength from the ground electronic state while the dark state governs the dissociation dynamics and the final state distribution.

If we only consider the two most strongly mixed bound states for each level, then the eigenstates can be written as follows.

$$\psi_1 = \alpha\psi_b + \beta\psi_d,$$
$$\psi_2 = -\beta\psi_b + \alpha\psi_d. \qquad (17)$$

Here ψ_b and ψ_d correspond to the zero-order bright and dark states, respectively, while ψ_1 and ψ_2 are the two bound eigenstates that share most of the oscillator strength. The intensities of transitions to ψ_1 and ψ_2 are proportional to α^2 and β^2, respectively, while the linewidths are proportional to β^2 and α^2. For $v' = 10$, this analysis leads to $\alpha = 0.85$ and $\beta = 0.53$; for $v' = 11$, $\alpha = 0.94$, $\beta = 0.35$. In a previous communication,[24] we showed that these results are consistent with IVR in the sparse limit. It will be interesting to determine how sensitive these results are to the details of the potential and to the initial value of v'. Since the dark state determines the dissociation dynamics, the final rotational state distribution of Cl$_2$ will depend on which particular λ state is coupled by IVR to the bright state. This should be a strong function of the potential.

Since the mixing between the bright and dark state, and the identity of the dark state, will not depend on v' in a simple way, there will not be an obvious trend of the IVR rate vs the initial v' state. For the present potential, the lifetime for $v' = 11$ is longer than for $v' = 10$ since the $v' = 10$ bright and dark states are more strongly mixed. We thus expect an erratic behavior of the lifetime as a function of v'.

1. Characterization of the initial metastable state

In order to assign the dark states ψ_d to specific levels $(v' - 1, \lambda)$ within the van der Waals manifold, we have performed quasibound state calculations using the same procedure as for calculating the ground state of Ar···Cl$_2$ [Eqs.

TABLE IV. Calculated rotational distributions of Cl$_2$ fragments in the vibrational predissociation of Ne···Cl$_2(B,v' = 11,\mathcal{G})$.

		$\Delta v = -1$		$\Delta v = -2$	
		Converged calculation	$\|\Delta v\| > 1$ coupling cut off	Converged calculation	$\|\Delta v\| > 1$ coupling cut off
Σ		94.7042	94.8601	4.9412	4.8237
$j =$	0	11.0106	11.0016	9.4885	9.1855
	2	13.2042	13.1985	14.3509	14.2925
	4	14.4290	14.4323	14.4795	14.4507
	6	14.6302	14.6340	13.0723	12.6673
	8	11.1989	11.1971	12.3350	12.1764
	10	8.6426	8.6427	9.2289	9.5022
	12	8.2007	8.2042	7.7978	7.9913
	14	5.8919	5.8899	6.8250	7.1959
	16	3.4137	3.4099	3.7537	4.1156
	18	3.6097	3.6114	2.8678	2.9380
	20	3.8330	3.8386	2.7066	2.6368
	22	1.9035	1.9073	1.3402	1.2383
	24	0.0321	0.0322	0.8446	0.7280
	26			0.4998	0.4692
	28			0.2042	0.1986
	30			0.1451	0.1466
	32			0.3399^{-1}	0.4057^{-1}
	34			0.2374^{-1}	0.2314^{-1}
	36			0.1715^{-2}	0.2770^{-2}
	38			0.5690^{-3}	0.6568^{-2}

(2)–(6)]. Since the $(v',\mathcal{G})$ level is mixed with $(v < v',\lambda)$ levels with a high value of λ, we had to use a different basis set in order to reach convergence: R_0 (Eq. 4) is taken as 4.5 Å instead of 3.7 Å for the harmonic oscillator basis, and no intermediate bending basis set is used. Thirty harmonic oscillator ($\omega = 15$ cm⁻¹), 20 free rotor, and 4 Cl₂ stretch basis functions ($v' + 1$, $v',v' - 1$, and $v' - 2$) were needed in order to achieve convergence. The results are listed in Table V.

TABLE V. (a) Position, width, and analysis of the resonances in the vibrational predissociation of Ar···Cl₂$(B,v' = 6,\mathcal{G})$. (b) Position, width, and analysis of the resonances in the vibrational predissociation of Ar···Cl₂$(B,v' = 10,\mathcal{G})$. (c) Calculated rotational distributions of Cl₂ fragments in the vibrational predissociation of Ar···Cl₂$(B,v' = 11,\mathcal{G})$.

(a)	2Γ (cm⁻¹)	τ (ps)	Energy (cm⁻¹)
Line shape	2.06×10^{-3}	2600	−178.288 20
Bound state			−178.322 11

(b)	2Γ (cm⁻¹)	τ (ps)	Energy (cm⁻¹)	% ψ_b	% $v'=10$	% $v'=9$	% $v'=8$
ψ_1 Line shape (reduced basis set) $v' = 10,$	0.058	91	−177.28	0.72			
$\mathcal{G}$ Bound state			−177.317		100		
$v' = 11, 10, 9, 8$ Bound state			−177.297		64	35	1
ψ_2 Line shape (reduced basis set) $v' = 9$ $\lambda = 36$	0.166	32	−176.69	0.28			
Bound state $v' = 11, 10$ $9, 8$			−176.955			100	
Bound state			−176.753		31	57	12
ψ_3 Line shape (reduced basis set) $v' = 9$ $\lambda = 35$	0.06	88	−177.95	<1%			
Bound state $v' = 11, 10$ $9, 8$			−178.002			100	
Bound State			−177.956		0.3	79	21

(c)	2Γ (cm⁻¹)	τ (ps)	Energy (cm⁻¹)	% ψ_b	% $v'=11$	% $v'=10$	% $v'=9$
ψ_1 Line shape (fully converged	0.0211	251	−176.603 04				
Line shape (reduced basis set) $v' = 11,$	0.021	250	−176.599	0.85			
$\mathcal{G}$ Bound state			−176.976 38		100		
$v' = 12, 11$ $10,9$ Bound state			−176.612 83		86	11	4
ψ_2 Line shape (reduced basis set) $v' = 10,$ $\lambda = 29$	0.18	29	−177.63	0.15			
Bound state $v' = 12, 11,$ $10, 9$			−177.6058			100	
Bound state			−177.620 63		10	80	10

It can be seen that there is one quasibound state correspond-
ing to each resonance, both for $v' = 11$ and $v' = 10$. Their
energies are quite well reproduced (they fall within one
linewidth of the corresponding resonance) as the mixing co-
efficients. For example, the resonance at -177.28 cm^{-1} for
$v' = 10$, which was shown from the model described in Eq.
(17) to be 72% ($\alpha^2 = 0.72$) of the bright state ψ_b [mainly
$(v' = 10, \mathcal{g})$] and 28% ($\beta^2 = 1 - \alpha^2 = 0.28$) of the dark
state $\psi_d (v' < 10)$, is found to be at -177.297 cm^{-1} and to
consist of 64% $v' = 10$, 35% $v' = 9$, and 1% $v' = 8$. The
projections of the corresponding wave function on $v' = 10$
and $v' = 9$ are shown in Fig. 10.

The other resonance at -176.69 cm^{-1} (28% ψ_b, 72%
ψ_d), is found at -176.75 cm^{-1} and is a superposition of
31% $v' = 10$, 57% $v' = 9$, and 12% $v' = 8$. The projections
of the corresponding wave functions on $v' = 10$ and $v' = 9$
are very similar to those shown in Fig. 10. These two levels
can be assigned as a combination of two zero-order states:
$(v' = 10, \mathcal{g})$ and $(v' = 9, \lambda = 36)$, with energy -177.317
cm^{-1} and -177.606 cm^{-1}, respectively, with a mixing co-
efficient of 31%–35%. Again, these zero-order state wave
functions are very similar to those plotted in Fig. 10. Unfor-
tunately, the pattern of the wave function of the
$(v' = 9, \lambda = 36)$ level is too complicated to allow for a

stretch/bend assignment of the excitation in the van der
Waals modes. (Here, $\lambda = 36$ means the 36th level of the van
der Waals manifold built with even j's, i.e., the 35th excited
even j level of $v' = 9$.)

In the case of $v' = 11$, the $(v' = 11, \mathcal{g})$ zero-order level
mixes principally with the $(v' = 10, \lambda = 29)$ level (λ has the
same meaning as for $v' = 11$). Contour plots of the wave
functions for the two zero-order states are shown in Fig. 11.
Again, the zero-order dark state is too complicated to be
given a simple bend–stretch assignment, although the nodal
pattern is somewhat simpler than the one of the
$v' = 9, \lambda = 36$ dark state. It is interesting that for both of the
doorway states the wave function has a considerable ampli-
tude at the linear configuration of the complex.

2. Characterization of the IVR regime

After assigning the $(v' = 10, \lambda = 29)$ dark state as the
doorway state for the $(v' = 11, \mathcal{g})$ bright state dynamics, a
golden rule calculation of the dissociation of the zero-order
dark state was performed, using Eq. (16). $\Psi_i^{(0)}$ was the zero-
order quasibound wave function of $(v' = 10, \lambda = 29)$, $\Psi_{fvjE}^{(0)}$
the continuum wave function corresponding asymptotically
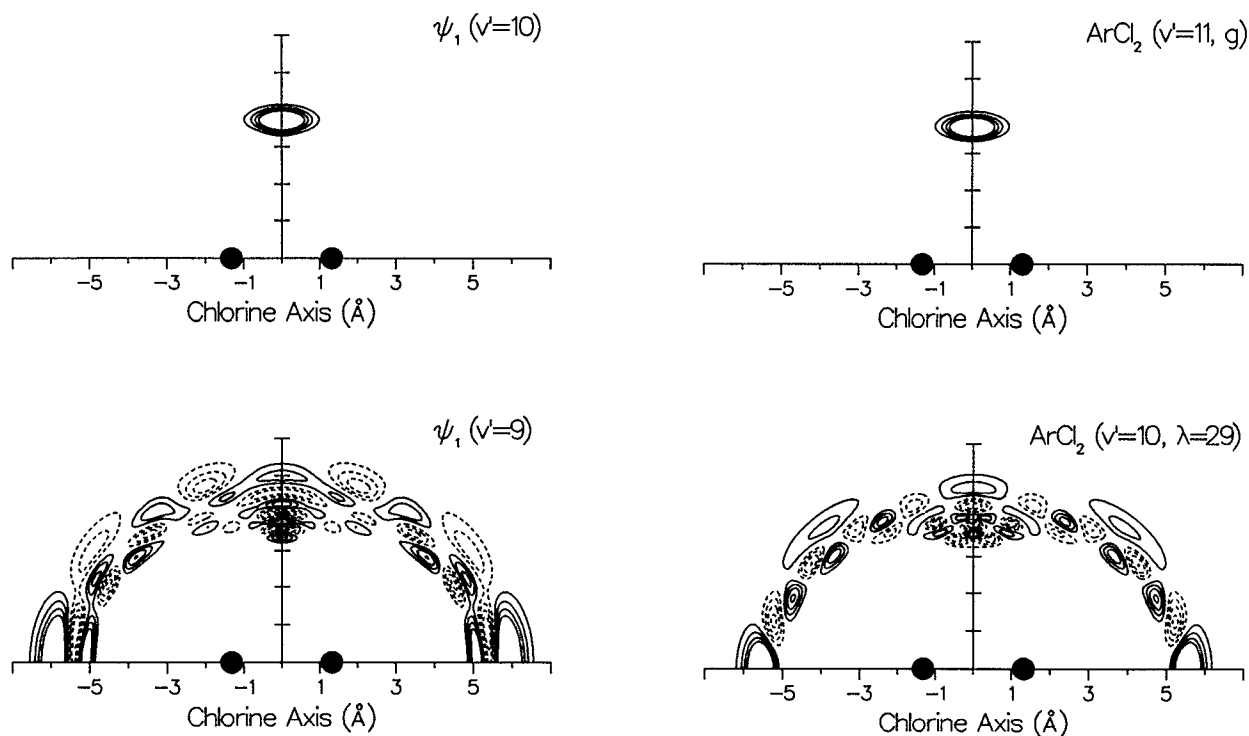to $Ar + Cl_2 (B, v < 10, j)$, and the product state distribution

FIG. 10. Wave function of the quasibound eigenstate ψ_1 for $v' = 10$, as de-
fined in Eq. (17), and calculated with 4 Cl_2 vibrational basis functions
($v = 11, 10, 9, 8$). The upper plot is the renormalized projection of ψ_1 onto
the vibrational component $v' = 10$ of Cl_2, and the lower plot onto $v' = 9$.
The same plots for ψ_2 are almost identical, as are the wave functions for
$(v' = 10, \mathcal{g})$ and for $(v' = 9, \lambda = 36)$, calculated with only one vibrational
channel of Cl_2. These plots support the assignment of ψ_b as $(v' = 10, \mathcal{g})$ and
ψ_d as $(v' = 9, \lambda = 36)$. However, the pattern of the $(v' = 9, \lambda = 36)$ wave
function is not assignable to any simple combination of van der Waals
stretching and bending excitation.

FIG. 11. Wave function of the zero order bright ψ_b $(v' = 11, \mathcal{g})$ (upper)
and dark $\psi_d (v' = 10, \lambda = 29)$ (lower) states involved in IVR from $v' = 11$.
The renormalized projections of ψ_1 and ψ_2 quasibound eigenstates calculat-
ed with 4 vibrational basis functions ($v = 12, 11, 10, 9$) onto $v' = 11$ and
$v' = 10$ gave the same wave function as the upper and lower plot, respective-
ly. These plots support the assignment of ψ_b and $(v' = 11, \mathcal{g})$ and ψ_d as
$(v' = 10, \lambda = 29)$. However, the pattern of the $(v' = 10, \lambda = 29)$ wave
function is not assignable to any simple combination of van der Waals
stretching and bending excitation.

$\Gamma_{vj}(E)$ and predissociation width $\Gamma(E)$ were calculated at the energy of the zero-order ($v' = 10, \lambda = 29$) dark state. As shown in Fig. 5 the golden rule rotational distribution is very similar to the result of the exact calculation for the bright state. The linewidth is 0.18 cm^{-1}, which is of the same order as the width of the dark resonance ($2\Gamma = 0.14$ cm^{-1}) obtained in the golden rule characterization of the continuum, and as the width of the dark state deduced from Table V(c) ($2\Gamma_d = 0.18/\alpha^2 = 0.21$ cm^{-1}). This gives a direct confirmation of the hypothesis of Evard *et al.*[5] that the product rotational distribution for $\Delta v = -2$ dissociation of Ar···Cl₂ is determined by the dynamics of the doorway state. As was the case for Ne and He···Cl₂, and for Ne and He···ICl, this rotational distribution is quite different from the decomposition of the quasibound state in terms of free rotor wave functions.

The magnitude of the coupling between the bright and dark states is given by $V = \alpha\beta\Delta E$, where α and β are the coefficients of Eq. (17) and ΔE is the energy spacing between the resonances corresponding to the quasibound eigenstates ψ_1 and ψ_2 (i.e., the energy difference between the resonances in the spectrum), $V = 0.27$ cm^{-1} for $v' = 10$ ($\alpha = 0.85, \beta = 0.53, \Delta E = 0.59$ cm^{-1}) and $V = 0.37$ cm^{-1} for $v' = 11$ ($\alpha = 0.92$, $\beta = 0.39$, $\Delta E = 1.03$ cm^{-1}) for the coupling potential responsible for IVR. The density of the ($v' - 1, \lambda$) levels, ρ, in the region of the ($v', \mathscr{g}$) state is approximately 0.7 levels/cm^{-1} and 0.5 levels/cm^{-1} for $v' = 10$ and 11, respectively. This give $\rho V \simeq 0.2$ for both levels, indicating that they correspond to the sparse limit for IVR. For $\rho V \ll 1$ we get the Fermi resonance limit, i.e., accidental resonance between a bright and a dark state, and for $\rho V \gg 1$ we get the dense limit for IVR, where the dark levels that are effectively coupled to the zero-order bright state build a quasicontinuum and give the bright state an IVR width which can be larger than the vibrational predissociation width. It would be quite interesting to look for these different regimes in Ar···Cl₂ or other similar complexes. Going to higher values for v', the density levels will be decreasing but the coupling should be increasing since the vibrational levels of Cl₂ are closer together.

C. Product rotational distribution: Dependence on the potential

Figures 4 and 5 show that, while the calculations do not quantitatively reproduce the measured product rotational distributions, they do reproduce the qualitative features observed in the experiments. Unlike dissociation of He···Cl₂ and Ne···Cl₂ which produced very smooth product rotational distributions, dissociation of Ar···Cl₂ produced highly structured distributions. This feature is reproduced well in the calculations. Vibrational predissociation from Ar···Cl₂($v' = 11$) is calculated to produce rotational distributions that are sharply peaked at $j = 10$ and 24. The calculated distributions are more sharply peaked than the measured distributions for this level, and the measured distributions peak at $j = 4$ and 22. However, the measured distributions tended to get sharper as the initial rotational state selectivity was increased. A truly state selected experiment might result in a measured distribution as sharp as those calculated here.

Another feature of the experiment that is nicely reproduced in the calculation is that the product rotational distributions are quite different for different initial vibrational levels. In addition, the calculation also predicts that $\Delta v = -2$ and $\Delta v = -3$ dissociation processes lead to very different product rotational distributions, unlike the very similar distributions observed in the analogous processes for He···Cl₂ and Ne···Cl₂. So far, no distributions have been measured for $\Delta v = -3$ dissociation of Ar···Cl₂.

The fact that the calculated distributions are quite different from the measured ones indicates that the potential used in the calculations is not correct. Although the atom–atom form for the potential used here worked well for He···Cl₂ and Ne··Cl₂, there are several reasons to expect that a more flexible form will be necessary for Ar···Cl₂. Most importantly, the correct potential for Ar···Cl₂ may have a minimum in the linear configuration as well as in the"T-shape" configuration. The polarizability anisotropy of Cl₂ favors the linear minimum at long range. Tao and Klemperer[25] performed Møller–Plesset (MP4) calculations for Ar···Cl₂ using a 6-31 + $G(2df)$ basis set and found that the linear minimum is preferred even for the equilibrium separation. With this basis set however, the superposition error is too large to draw a definite conclusion.

Since the IVR product rotational distributions are highly structured, they will provide a rigorous test of any assumed potential. In the future, rotationally state-selected experiments should be performed to provide data for such a test. In this regard, it is especially useful that the golden rule approximation can be used to obtain approximate results for the product state distributions. This fact, which was not anticipated, will allow for a considerable savings in computer time in the search for an accurate surface.

VI. SUMMARY AND CONCLUSIONS

Exact calculations have been performed for the excitation line shapes and dissociation dynamics of the Ar···Cl₂, B state, $v' = 6$ and 11 levels. Smaller basis set calculations, over larger energy ranges, were performed for $v' = 10$ and 11. The IVR mechanism for $\Delta v = -2$ dissociation of Ar···Cl₂ has been unambiguously confirmed. For a given potential, the dark, doorway states can be identified, and the mixing strengths can be calculated. For the $v' = 10$ and 11 bright states, the dark states are the 36th and 29th, respectively, even van der Waals vibrational levels in the $v' - 1$ manifold. These levels are highly excited and mixed, and therefore no simple bend–stretch assignment is possible. If similar calculations were performed for high v' levels, then the dark state would be expected to be lower in the $v' - 1$ manifold, and might be assignable. It was also shown that approximate calculations based on quasibound states coupled via the golden rule to the continuum are qualitatively accurate. This is true even though the Cl₂ zero-order states are highly mixed because the bound–continuum coupling responsible for dissociation remains weak, even if the bound–bound interaction responsible for IVR is quite important. Another factor is that the resonance widths are

much less than the level spacing.

The dissociation dynamics of Ar···Cl₂ are especially interesting because they fall between the direct bound–free limit that is characteristic of He···Cl₂ and Ne···Cl₂ and the statistical limit that appears to apply to Kr···Cl₂ and Xe···Cl₂. The dissociation dynamics of the Ar···Cl₂ B state will be a strong function of the initial Cl₂ stretching level. For $v' < 8$, $\Delta v = -1$ is open, but dissociation is quite slow because of the heavy Ar mass. For $v' = 6$, the dissociation lifetime is calculated to be 2.5 ns even though the energy gap is only 18 cm^{-1}. For $v' > 8$ the dynamics proceed via IVR in the sparse limit. One, or only a few, doorway states provide the path from the initial quasibound state to the continuum. Since the energy mismatch and the coupling between the bright and dark states will be different for every initial level, it is not possible to predict how the dynamics will vary as a function of the initial state quantum numbers without performing the full calculation with an accurate potential. For the potential used here, for instance, the $v' = 11$ bright state lifetime is three times as long as the $v' = 10$ lifetime, and 1/30 times as long as the $v' = 6$ lifetime, in direct contradiction of the energy gap law.

Calculations such as those reported here will provide a severe test for any assumed potential. While the atom–atom Morse–van der Waals form of the potential employed here was adequate to reproduce the dissociation dynamics for He···Cl₂ and Ne···Cl₂, it is not sufficient for Ar···Cl₂ even though it contains the right well depth and geometry of the initial level. The calculated rotational distributions will be very sensitive to the assumed anisotropy since it is required that exactly the correct bend–stretch van der Waals level of the dark manifold be in near resonance with the bright state. Since these calculations are quite expensive, even with the reduced basis set, it may be wise to wait for state resolved data before extensive data fitting is performed. A final important result of these calculations is that the intensity borrowing by the dark states is extensive enough that they may be directly observable if the rotational manifold can be sufficiently cooled to relieve congestion of the excitation spectrum. A related result is that the lifetime measured in a time resolved experiment on this and similar species[26] will be quite dependent on the excitation bandwidth. Since the observed lifetime will depend on the extent to which both the bright and dark states are excited, it will be necessary to study the spectroscopy of species in detail before measured lifetimes can be interpreted.

ACKNOWLEDGMENTS

[1] J. A. Beswick, G. Delgado-Barrio, and J. Jortner, J. Chem. Phys. **70**, 3895 (1979); J. A. Beswick and J. Jortner, Adv. Chem. Phys. **47**, 363 (1981); O. Roncero, J. Campos-Martinez, A. M. Cortina, P. Villarreal, and G. Delgado-Barrio, Chem. Phys. Lett. **148**, 62 (1988); G. E. Ewing, J. Chem. Phys. **71**, 3134 (1979).

[2] J. A. Blazy and D. H. Levy, J. Chem. Phys. **69**, 2901 (1978); W. Sharfin, P. Kroger, and S. C. Wallace, Chem. Phys. Lett. **85**, 81 (1982).

[3] J. I. Cline, D. D. Evard, B. P. Reid, N. Sivakumar, K. C. Janda, and N. Halberstadt, J. Chem. Phys. **89**, 3535 (1988).

[4] J. I. Cline, N. Sivakumar, D. D. Evard, C. R. Bieler, B. P. Reid, N. Halberstadt, and K. C. Janda, J. Chem. Phys. **90**, 2606 (1989).

[5] D. D. Evard, C. R. Bieler, J. I. Cline, N. Sivakumar, and K. C. Janda, J. Chem. Phys. **89**, 2829 (1988).

[6] C. R. Bieler, K. E. Spence, and K. C. Janda, J. Phys. Chem. **95**, 5058 (1991).

[7] K. C. Janda and C. R. Bieler, *Atomic and Molecular Clusters*, edited by E. Bernstein (Elsevier, New York/Amsterdam, 1990).

[8] R. L. Waterland, J. M. Skene, and M. I. Lester, J. Chem. Phys. **89**, 7277 (1988).

[9] J. C. Drobits and M. I. Lester, J. Chem. Phys. **86**, 1662 (1987).

[10] N. Halberstadt, J. A. Beswick, and K. C. Janda, J. Chem. Phys. **87**, 3966 (1987).

[11] R. L. Waterland, M. I. Lester, and N. Halberstadt, J. Chem. Phys. **92**, 4261 (1990).

[12] O. Roncero, J. A. Beswick, N. Halberstadt, P. Villarreal, and G. Delgado-Barrio, J. Chem. Phys. **92**, 3348 (1990).

[13] S. K. Gray and C. E. Wozny, J. Chem. Phys. **94**, 2817 (1991).

[14] N. Halberstadt, R. Schinke, and J. A. Beswick, in *Half Collision Resonance Phenomena in Molecules*, AIP Conference Proceedings **225**, edited by M. García Sucre, G. Raseev, and S. C. Ross (AIP, New York, 1991).

[15] M. Heppener, A. G. M. Kunst, D. Bebelaar, and R. P. H. Rettschnick, J. Chem. Phys. **83**, 5341 (1985).

[16] J. A. Coxon, J. Mol. Spectrosc. **82**, 265 (1980).

[17] W. Lester, Methods Comput. Phys. **3**, 322 (1968); **10**, 243 (1971).

[18] B. P. Reid, K. C. Janda, and N. Halberstadt, J. Phys. Chem. **92**, 587 (1988).

[19] K. P. Huber and G. Herzberg, *Molecular Spectra and Molecular Structure IV, Constants of Diatomic Molecules* (Van Nostrand Reinhold, New York, 1979).

[20] The rotational channels were distributed as follows: $v = 3$: 30; $v = 4$: 25; $v = 5$: 25; $v = 6$: 20; $v = 7$: 20.

[21] The rotational channels were distributed as follows: $v = 7$: 30; $v = 8$: 30; $v = 9$: 25; $v = 10$: 25; $v = 11$: 25; $v = 12$: 25; $v = 13$: 20.

[22] The rotational channels were distributed as follows: $v = 6$: 30; $v = 7$: 30; $v = 8$: 30; $v = 9$: 25; $v = 10$: 25; $v = 11$: 25; $v = 12$: 25; $v = 13$: 20.

[23] The distribution of the rotational channels was as follows: $v' - 3$: 30; $v' - 2$: 25; $v' - 1$: 25; v': 25; $v' + 1$: 25; $v' + 2$: 20.

[24] N. Halberstadt, J. A. Beswick, O. Roncero, and K. C. Janda, J. Chem. Phys. **96**, 2404 (1992).

[25] F. M. Tao and W. Klemperer (to be published).

[26] D. M. Wilberg, M. Gutmann, J. J. Breen, and A. H. Zewail, J. Chem. Phys. **96**, 198 (1992).